FRAGMENTATION EXPERIMENTS FOR THE EVALUATION OF THE SMALL SIZE DEBRIS POPULATION

Wolfgang Fucke

Battelle Ingenieurtechnik GmbH, Frankfurt am Main, Germany

ABSTRACT

ESA/ESOC currently develops a space debris reference model for the long term prediction of the space debris population. In order to obtain characteristic data of debris generated in explosions we performed model experiments with downscaled ARIANE 4 H10 tanks (1:5 in diameter and 1:10 in length). Scaling rules for the tank and the generated debris are discussed. A scenario derived by us demonstrates that a detonation of the H_2-O_2-content is conceivable; so we addressed to detonative rupture. Two of the three experiments were performed at low temperature (-45°C). The velocity of the fragments was measured, and the fragments were softly recovered. The mass distribution is compared to that of the Atlas-test. In the time span of observation the fragments did not reach their final velocity. The evaluation is not yet finished.

1. INTRODUCTION

A detailed knowledge of the present and future space debris population is necessary for the assessment of the collision risk of space missions and for the design of protection shields. As measured data of the actual debris environment are necessarily incomplete especially for particles smaller than 5 to 10 cm, and as they do not allow to predict the future development of the debris environment, only a mathematical model which contains the sources and sinks of all objects in space is able to fulfil the requirements.

Such a model called "ESA Reference Model for Space Debris and Meteoroids" is currently developed for ESA/ESOC in a joint program of Technical University Braunschweig (TUBS-IfRR, Prof. Rex) and Battelle. The establishment of the model is performed by TUBS-IfRR and is presented in a different paper (Ref.1). Battelle's work is addressed to the consolidation of model data by on-ground experimental simulation of fragmentation events. In this paper a preliminary overview of the experiments will be given, since the study is not yet finished.

2. DATA GAPS

The most essential sources of man-made space debris are explosions of spacecraft. They cover about 97% of all recorded fragmentation events in space. In literature only few explosion experiments dedicated to the evaluation of debris characteristics can be found. The best known of them is the Atlas tank fragmentation (Ref.2). Moreover, the fragmentation of steel shells filled with high explosive and of ground based gas pressure vessels has been examined. Mass distribution formulae have been derived from this poor data base, but there is no information about fragment velocities or size distributions.

We therefore concentrated on explosion experiments with a representative spacecraft structure in order to obtain information about fragmentation and the debris characteristics.

3. TYPES OF EXPLOSIONS

With the term "explosion" a very fast rupture of a structure caused by an internal pressure is described. This definition comprehends a variety of phenomena occurring in different pressure and velocity regimes and is therefore vague. Principally one has to distinguish between **physical** and **chemical** explosions.

In a **physical explosion** the pressure in a closed vessel slowly rises until the burst pressure is exceeded. The pressure rise can e.g. occur due to heating of the content when a pressure relief valve fails to function. Because no transient stresses occur, the vessel typically only tears along lines of weakness. So, if any, only few fragments are generated. The additional velocities are low.

In a **chemical explosion** the pressure rises due to a fast chemical reaction of a fuel mixture. The reaction requires an appropriate ignition source. The explosion pressure p_{ex} which is obtained after completion of the reaction exceeds the initial pressure p_i significantly (e.g. $p_{ex}/p_i = 9$ for a stoichiometric GH_2 - GO_2 mixture).

There are two different modes of energy release:

- In a **deflagration** the reaction zone ("flame front") travels with subsonic speed. So pressure waves can run into the unburned fuel in front of the flame front. The pressure rises from p_i to p_{ex} in a millisecond scale. Flame front velocity and pressure rise time depend on the mixture, the vessel geometry, and the ignition conditions, and may vary with time. Hot particles or surfaces as well as electrical sparks serve as ignition source.

- A **detonation** is an extremely fast reaction connected to a strong shock wave ("detonation wave"). The very high transient pressure p_{Det} exceeds p_{ex} significantly. Its rise time lies in the microsecond scale. The detonation speed D is supersonic and depends only on type and state of the mixture. For a stoichiometric GH_2-GO_2 mixture at atmospheric pressure holds $p_{Det}/p_i = 27$ and $D \approx 2800$ m/s (Ref.3).

  A detonation can directly be initiated only by a strong shock wave as it is generated by a high explosive (e.g. in a blast cap). A deflagration to detonation transition (DDT) is possible when structures in the tank lead to a turbulent flow acceleration ahead of the flame front, or when the pressure waves from multiple ignition points interact.

Generally, the degree of fragmentation of an exploding structure depends on the pressure rise time and amplitude. The shorter the time available for pressure, stress, and shear waves to compensate locally induced pressure or stress fields, the smaller and faster are the fragments. Thus a detonation generates the most and smallest fragments, and the physical explosion the largest. The deflagration ranges in its intensity from a relatively slow reaction to nearly a

detonation, thus giving rise to different particle size and velocity distributions within these margins.

4. A Representative Tank Structure

In order to design a simplified model experiment a precise knowledge of the construction and the operating conditions of a representative tank is required. By support of ESA we got the opportunity to visit the plant where the ARIANE 4 upper stage tanks are built, and were informed about details of design and construction. So we selected this tank as the base for the model experiments.

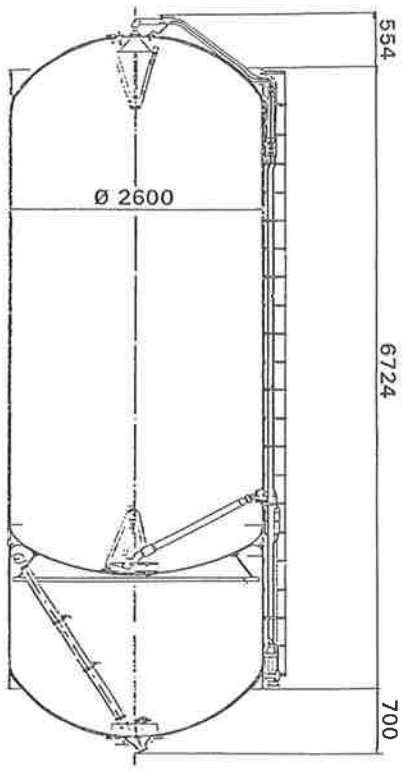

Figure 1 Design of the ARIANE 4 H10 tank

The cryogenic ARIANE 4 H10 tank has a total length of more than 7.5 m, a diameter of 2.6 m, and carries 10 t of fuel (Figure 1). By an inner bulkhead the tank is divided into the upper LH_2-tank and the lower LOX-tank. The cylindrical walls are constructed of aluminium alloy sheets which are welded together. The bulkheads are made of preformed and welded aluminium alloy segments. The inner common bulkhead consists of two such shells with an evacuated honeycomb structure in between. The whole construction is kept together by three rigid support rings. The thickness of the walls and the bulkheads ranges from 3 mm to considerably below 1 mm. For the thermal insulation 20 - 25 mm thick PVC-foam plates are glued to the outer surface of the tank.

5. In Orbit Explosion Scenario

Our experiments have to generate a statistically relevant number of fragments in the cm-range and smaller. As this can only be performed by a detonation, we concentrated on a detonation of the mixed content of a fuel tank.

Is a chain of events conceivable that leads to a detonation of a structure like the ARIANE 4 H10 tank?

After main engine cut off there is still some fuel remaining in the cells. Two safety valves keep the hydrogen and oxygen pressures below 3.15 bar and 2.35 bar respectively.

- The pressure in the LH_2-tank may decrease due to loss of LH_2 caused for example by a hole generated by the impact of a small particle or by a structural failure due to fatigue.
- When the constant LOX-pressure exceeds the LH_2-pressure by more than 0.2 bar a reversal of the common bulkhead becomes possible. The higher the differential pressure the more violent is the reversal process. The double shell structure breaks, some aluminium parts are released, and the brittle honeycomb structure is fragmented mainly into small size debris.
- Now oxygen flows into the LH_2-tank and turbulently mixes with the hydrogen. The violence of the flow depends on the differential pressure at bulkhead rupture.
- By reaction with oxygen the fresh aluminium surfaces are heated up. Part of the probably burning GRP debris of the honeycomb structure is blown into the LH2-tank by the oxygen flow. So there exist several potential sources for the ignition of a deflagration which then will rupture the LH_2-tank.
- By the turbulences generated during the passage of the oxygen through the broken bulkhead or by interaction of the pressure waves from multiple ignition points finally even a DDT may occur.

Fragments of the brittle insulation are generated by all events following a bulkhead rupture. Their number and velocity increase, and their size decreases with the violence of the event.

All attached structures as there are for example fuel tubes and the different parts of the thrust device can also be torn off by all types of event. It is not to be expected, however, that they will be broken down into small size debris.

6. Scaling of the Model Tank

As the planned explosion experiments cannot be performed in full scale the proper scaling has to be guaranteed.

In a thin walled cylindrical pressure vessel the same stress and strain states occur when the 'pressure vessel formula' yields the same value of A which is specific for the material of the vessel wall:

$$\frac{p \cdot r_0}{d} = A \qquad (1)$$

where
- p overpressure
- r_0 radius of the cylinder
- d wall thickness of the cylinder

Hence, for correct scaling not only the geometric dimensions but also the pressure can be utilized.

For the ARIANE 4 H10 LH_2-tank under functional load conditions with an average wall thickness of 2 mm one gets $A = 2.05 \cdot 10^8$ *bar*. This value has to be kept constant during scaling.

Figure 2 shows the relationship of tank radius and overpressure for different wall thicknesses. The operating pressure and the radius of the full scale tank are indicated by dashed lines.

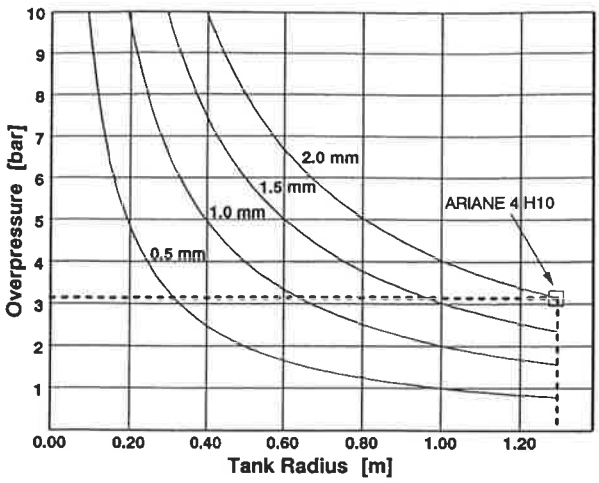

Figure 2 Overpressure p of a scaled A4 H10 hydrogen tank as function of the tank radius r_0 for different wall thicknesses d

The wall thickness of the model tank should not be made thinner than 0.5 mm to avoid welding and stability problems. So the hyperbola for $d = 0.5$ *mm* is a limit curve. If the tank radius is chosen below 32.5 cm, the pressure has to be increased in excess of the full scale value of 3.15 bar.

diameter cm	scale	length cm	volume l	wall mm	press. bar	TNT kg
10,0	1:26,0	15,0	1,2	0,5	20,5	0,1
20,0	1:13,0	30,0	9,4	0,5	10,3	0,2
30,0	1:8,7	45,0	31,8	0,5	6,8	0,6
40,0	1:6,5	60,0	75,4	0,5	5,1	1,0
50,0	1:5,2	75,0	147,3	0,5	4,1	1,7
60,0	1:4,3	90,0	254,5	0,5	3,4	2,5
70,0	1:3,7	105,0	404,1	0,5	2,9	3,5
80,0	1:3,3	120,0	603,2	0,5	2,6	4,7
90,0	1:2,9	135,0	858,8	0,5	2,3	6,2
100,0	1:2,6	150,0	1178,1	0,5	2,1	7,9
260,0	1:1,0	390,0	20706,2	2,0	3,2	144,3

Table 1 Scaling of the ARIANE 4 H10 tank

In Table 1 the most important data of model tanks with different diameters and constant wall thickness are given. The vessel length is 1.5 times the diameter. We believe that this is about the shortest length where influences of the bulkheads on the rupture behaviour will not dominate. The last two columns of the table give the scaled overpressure and the corresponding TNT-equivalent of a stoichiometric H_2-O_2-mixture. The data of the full scale tank with reduced length are also shown. The TNT-equivalent increases with decreasing temperature (e.g. by 30% at -40°C).

For the experiments, the TNT-equivalent is a governing parameter and has to be kept as small as possible. In order not to exceed 2 kg we decided to design a model tank with a diameter of 50 cm. The corresponding row in table 1 is marked by arrows.

7. Scaling of the Fragments

Which influence has the scaling of the vessel on the size and the velocity of the debris?

The explosion pressure p_{expl} accelerates the tank wall into radial direction. Neglecting strain work (because the wall is very thin) the equation of motion for the expanding cylinder wall is obtained as:

$$\ddot{r} = \frac{p_{expl}}{\rho_w \cdot d} \tag{2}$$

where r radius of the cylinder ($r=r_0$ for $t=t_0$)
p_{expl} explosion pressure
ρ_w density of the cylinder wall
d thickness of the cylinder wall

The cylinder wall ruptures when the maximum elongation ϵ_{max} is reached:

$$\frac{r - r_0}{r_0} = \epsilon_{max}$$

For the acceleration phase a constant pressure can be assumed. From $t = \sqrt{2 \cdot (r - r_0) / \ddot{r}}$ follows the rupture time:

$$t_{rupt} = \sqrt{2 \cdot \epsilon_{max} \cdot \rho_w \cdot \frac{r_0 \cdot d}{p_{expl}}} \tag{3}$$

and with $\dot{r} = \ddot{r} \cdot t$ the expansion velocity at rupture:

$$v_{rupt} = \sqrt{\frac{2 \cdot \epsilon_{max}}{\rho_w} \cdot \frac{p_{expl} \cdot r_0}{d}} \tag{4}$$

Since p_{expl} is proportional to the initial pressure p the expansion velocity at rupture time t_{rupt} is the same for all vessels which have been scaled according to $p \cdot r_0/d$ (equation 1). This is the initial fragment velocity.

Also the subsequent acceleration of the fragments in the exhausting gas flow is governed by the scaling law, where p_{expl} determines the maximum acceleration force, r_0 the duration of the flow and d the inertial force of the fragment.

So, the fragment velocity is virtually independent of the scaling.

The pressure wave in the exploding gas induces local stress fields in the cylinder wall. This stress spreads along the cylinder wall with a certain velocity (shear wave velocity, stress wave velocity) which depends on the wall material and to a lesser extent on the stress amplitude. Thus, the size of the large fragments depends on the distance the stress waves can travel until the vessel ruptures. Because $p_{expl} \sim p$ and $p \sim d / r_0$ (from scaling), equation 3 yields:

$$t_{rupt} \sim r_0 \tag{5}$$

While thus the linear dimensions of so generated fragments scale with r_0, their total number is independent on the scaling factor. Because they have the total wall thickness, their mass scales with $r_0^2 \cdot d$.

The size of the larger debris from the thermal insulation should virtually follow the same rules because its fragmentation is governed by the fragmentation of the aluminium tank structure on which the insulation is fixed.

The distribution of the small size debris, that is the debris with smaller dimensions than the wall thickness, should be independent of the scaling factor, because it is generated locally in the vicinity of the breaks. Hence the geometry of

the vessel should have no essential influence on its size. Their total number, however, depends on the geometry due to the overall length of the breaks which scales with r_0.

8. Design of the Model Tank Structure

As it is not necessary to produce in the experiments the complete chain of events leading to a detonation the model tanks can have a drastically reduced complexity compared to the original tank structure. The following major reductions in complexity have been accomplished:

- Only the tank structure has been modelled, but no attached parts as there are the thrust device, fuel tubes etc.
- The interior structures of the tank and the common bulkhead have been omitted.
- The upper and lower bulkheads have been replaced by rigid plates (reduction to a pure cylinder geometry).

However, the thermal insulation at the outside of the cylinder wall was modelled in 2 of 3 experiments.

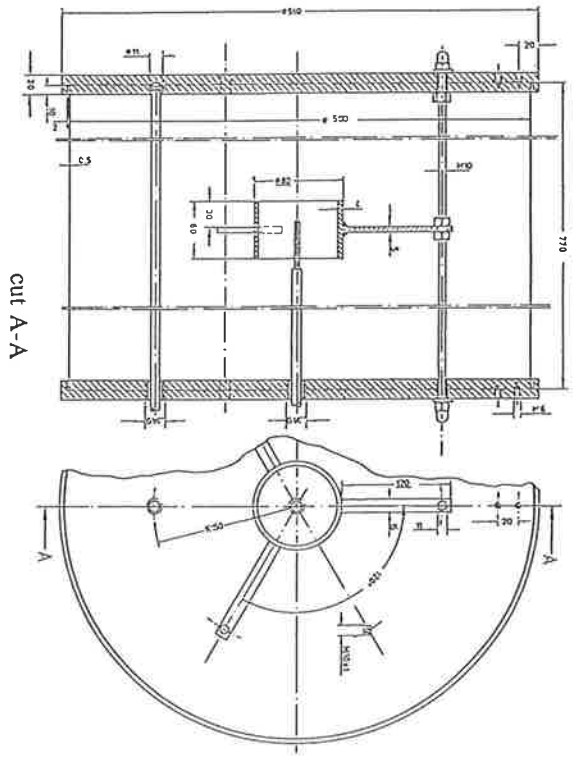

Figure 3 Sketch of the model tank

A sketch of the model tank is shown in Figure 3. The wall thickness is 0.5 mm (scale 1:4), the diameter 500 mm (scale 1:5.2) and the interior length 750 mm (scale near 1:10). The cylindrical body is closed by two 25 mm thick aluminium end plates which are clamped together by three 16 mm bolts. So the wall has not to sustain stresses from the end plates. The material of the wall is AlZnMg1 (W.Nr. 3.4335) which corresponds to the original material and has good low temperature properties. The wall was manufactured from one sheet welded together and to the end plates.

For the insulation 5 mm original PVC foam was glued to the cylinder with original epoxy resin.

The tank is filled with the two gases successively through the gas inlet tube which has a row of outlet holes directed to the tank wall in order to obtain a good mixing.

The tube in the centre of the cylinder carries the blast cap which is required for initiation of a detonation of the fuel mixture. Its debris is caught by a ring so that the wall will not be hit.

9. Diagnostics

Objective of the experiments was to measure the mass distribution and, as far as possible, the velocity distribution of the debris generated in explosions. For this purpose we applied two different diagnostic methods, namely the soft recovery of the fragments, and high speed camera and flash X-ray observation of their flight.

The model tanks were exploded in the centre of a steel tube of 1.5 m diameter and 1.5 m length. The axes of the tank and the tube were the same. The inside of the tube was coated with about 10 cm thick soft recovery material. It consisted of styrofoam, a paper felt stack and chipboard. In pre-tests with 0.5 g aluminium disks at about 100 m/s this combination had turned out to be the most efficient. The coating was divided into 120 fields.

After the explosion experiments the fragments were sampled and their mass distribution evaluated. The mass of construction elements (end plates, gas inlet tube, igniter tube and bolts) were not taken into account.

For the determination of the velocity of the fragments we used two different high speed cameras looking end on at the tank.

With the 16 mm film camera *HYSPEED* (maximum framing speed 10^4 frames/second) we recorded the complete ring space between the test tank and the steel tube. After the first shot, however, it turned out that the detonation light flash lasted longer than the flight time of the fragments to the soft catcher so that velocity measurement was not possible.

The electronic image converter camera *IMACON 790* has the advantage of a higher framing speed so that the motion blur is smaller, but has a minor resolution. So the field of view had to be reduced to a sector of the gap between tank and steel tube. We operated the camera at a framing speed of $5 \cdot 10^4$ frames per second (up to 16 frames). The resolution is 2.5 mm in the object plane, and the motion blur amounts to 0.8 mm for particle velocity 100 m/s. This camera was helpful in the early acceleration phase when the shell fragments still hide the detonation flash.

From the high speed film records only the radial component of the particle velocities can be obtained. By stripes of different colour painted on the tank and its insulation the origin of the softly recovered fragments can be localized. Origin, location of impact and radial velocity from the high speed cine records (if the particle can be assigned) yields the complete velocity vector of a specific particle.

The *HYSPEED* camera was replaced after the first experiment by flash X-ray equipment. From 3 X-ray shadowgraphs taken at different times two averaged velocities are obtained.

Besides, we measured inside of the vessel the temperature of the gas and its static pressure as well as the dynamic pressure during the explosion.

10. Experimental Parameters

In total we performed 3 explosion experiments, all with stoichiometric H_2-O_2-mixture. In all cases the surrounding of the tank was under atmospheric pressure which balanced part of the initial pressure in the tank. Aeroballistics cannot become effective in the short time of flight.

The main parameters of the three experiments were the following:

ESOC 1: tank without insulation
ambient temperature
initial absolute pressure 4.1 bar

ESOC 2: tank with insulation
temperature ≈ -45°C
initial absolute pressure 4.1 bar

ESOC 3: tank with insulation,
temperature ≈ -45°C
initial absolute pressure 5.1 bar

In the first two experiments we applied an initial pressure reduced by 1 bar mainly because we were afraid to destroy the soft recovery device by a too high amount of exploding gas. In view of the high detonation pressure the slightly reduced initial stress of the wall should be of minor influence on the fragmentation behaviour.

ESOC 1 served as reference experiment. As the aluminium alloy does not embrittle at those low temperatures that could be realized, cooling of the tank was not necessary. Cooling had, however, to be accomplished for *ESOC 2* and *ESOC 3* when a PVC-foam insulation was applied. By cooling with dry ice from outside we achieved -45°C of the gas content. We regard this as a representative average temperature of an orbiting tank.

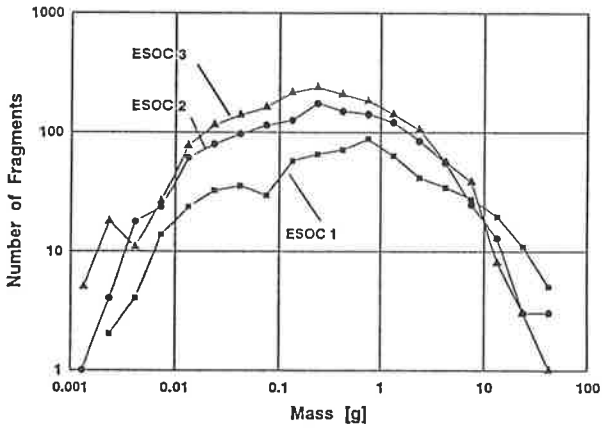

Figure 4 Number of fragments versus mass

For *ESOC 3* the initial pressure was raised to the value given by correct scaling. The according TNT-equivalent amounted to 2.2 kg.

It turned out with shot *ESOC 2* that it was not possible to recover the highly brittle insulation material because it was atomized during impact. In spite of this we applied the insulation also for shot *ESOC 3* in order to maintain the wall mass.

11. Results

The preliminary evaluation of the three shots has been nearly completed. The final analysis is currently on the way.

Figure 4 shows the number of aluminium fragments plotted as function of their mass. The three curves have a similar shape but are slightly shifted. *ESOC 1* has yielded 632 particles, *ESOC 2* 1302 particles, and *ESOC 3* 1762 particles. The maximum is at 0.73 g for *ESOC 1* and at 0.24 g for the other experiments. Particle sizes and number are conform with the rising energy content from *ESOC 1* to *ESOC 3*. The smallest particles found have a weight of 1 mg. About 99% of the mass have been recovered.

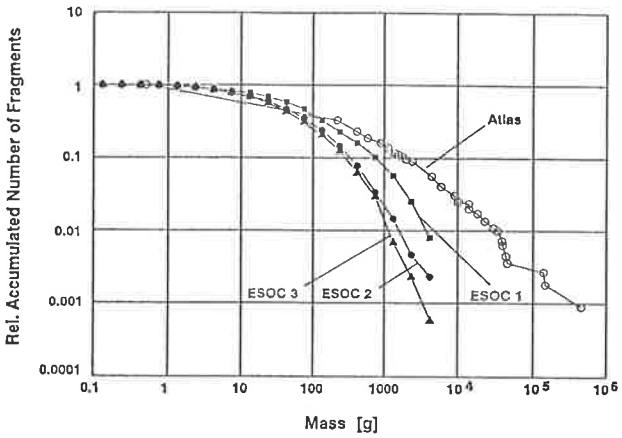

Figure 5 Accumulated number of fragments normalized to total number of fragments versus mass

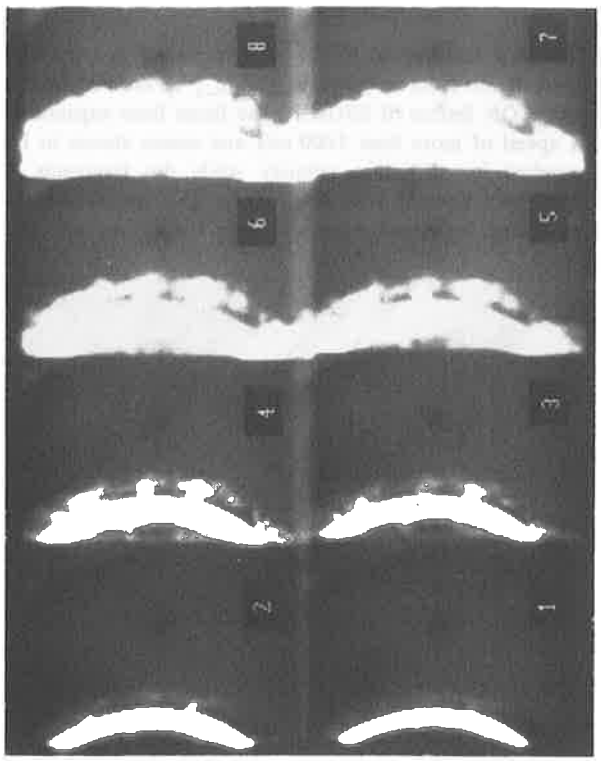

Figure 6 *IMACON* framing sequence of *ESOC 1*

In Figure 5 the accumulated fragment number normalized to the total fragment number is plotted versus the mass. In order to compare our results with the Atlas fragmentation test (Ref.2) we shifted our curves to higher masses by a factor of 100 according to the scaling with $r_0^2 \cdot d$ (see chapter 7). All four curves have similar shapes. According to the energy content the steepness of the slope rises from *ESOC 1* to *ESOC 3*; that means more and more smaller particles. The slower rise of the Atlas-curve indicates that the reaction might not have been a detonation. Additionally, the heavier fragments may partly have been attached aggregates which have not been modelled in our experiments.

The velocity of the individual fragments could not be measured. In Figure 6 a framing sequence of the *IMACON*-camera is shown. The time interval between the frames is 18 μs. The regular fragmentation of the wall and the elapsing gas jets are clearly visible.

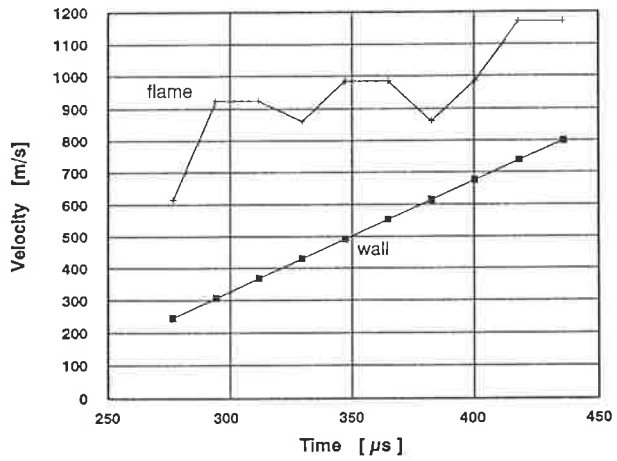

Figure 7 Velocity versus time for wall fragments and flame front of *ESOC 1*

The expansion speed of the wall fragments and the outermost flame front is given in Figure 7 as derived from the IMACON frames of *ESOC 1*. The flame front expands with a speed of more than 1000 m/s and seems almost to have reached its maximum velocity while the fragments still accelerate linearly with time. Their final speed cannot be estimated, but should be significantly higher than 800 m/s.

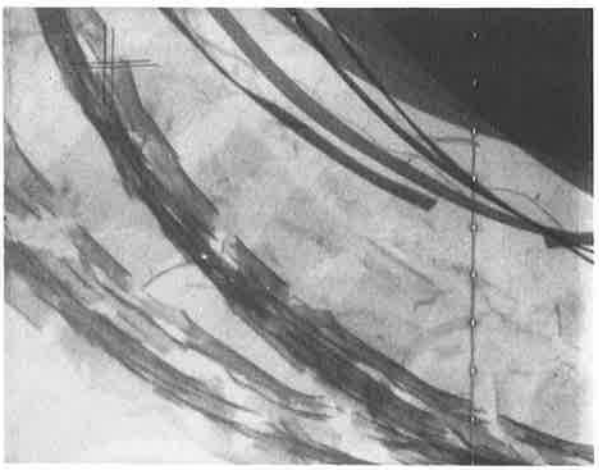

Figure 8 X-ray double exposure of the expanding tank wall of *ESOC 3*

For *ESOC 2* and *ESOC 3* we applied X-ray flashes. Part of the first double exposure of *ESOC 3* shows Figure 8. As before, the tank wall fragments very regularly and expands symmetrically. After correction of the parallax the velocity can be obtained. Results for *ESOC 2* are depicted in Figure 9. The symbols denote average velocities derived for different radial directions. The lines mark the upper and lower limit of the velocities when the uncertain axial positions of the fragments and the decreasing framing scale from front to back of the vessel are taken into account. The diagram contains also the dates of *ESOC 1* from figure 7. The velocity-time behaviour coincides well. Apparently the additional mass of the insulation is compensated by the higher energy content of *ESOC 2*.

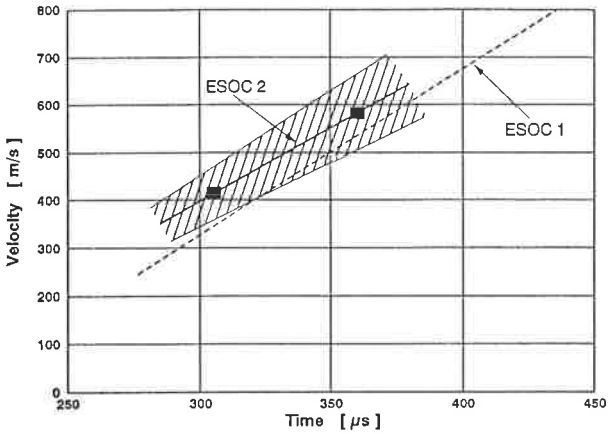

Figure 9 Velocity versus time for wall fragments of *ESOC 2* and *ESOC 1*

In all three experiments the particle velocities were independent of size and direction. Moreover, number and size of fragments showed no dependence on the flight direction. Significant axial velocity components could not be found so that our experiments exhibited a perfect cylindrical symmetry.

12. References

1. Sdunnus, H and Klinkrad, H., *An introduction to the ESA reference model for space debris and meteoroids*, First European Conference on Space Debris, Darmstadt, 5-7 April 1993

2. Bess,T.D., *Mass distribution of orbiting man made space debris*, NASA TN D-8108, Dec. 1975

3. Edwards, D.H., Williams, G.T. and Breeze, J.C., *Pressure and velocity measurements on detonation waves in hydrogen-oxygen mixtures*, J.Fluid Mech. **6** (1959) 497

13. Acknowledgments

This work has been sponsored by ESA-ESOC. The author wants to thank Dr. H. Klinkrad of ESOC and Mr. H. Sdunnus of TUBS-IfRR for the helpful discussions, and Mr. W. Haas and Mr. H. W. Bolloni for the ingenious performance of the experiments.